PHYSICAL REVIEW B **90**, 081104(R) (2014)

Bond order and the role of ligand states in stripe-modulated $IrTe_2$

K. Takubo,[1,2,3,*] R. Comin,[1,2] D. Ootsuki,[4] T. Mizokawa,[4,†] H. Wadati,[5] Y. Takahashi,[6] G. Shibata,[6] A. Fujimori,[6] R. Sutarto,[7] F. He,[7] S. Pyon,[8] K. Kudo,[8] M. Nohara,[8] G. Levy,[1,2] I. S. Elfimov,[1,2] G. A. Sawatzky,[1,2] and A. Damascelli[1,2,‡]

[1]*Department of Physics and Astronomy, University of British Columbia, Vancouver, British Columbia V6T 1Z1, Canada*

[2]*Quantum Matter Institute, University of British Columbia, Vancouver, British Columbia V6T 1Z4, Canada*

[3]*Max Planck Institute for Solid State Research, Heisenbergstrasse 1, D-70569 Stuttgart, Germany*

[4]*Department of Physics and Department of Complexity Science and Engineering, University of Tokyo, 5-1-5 Kashiwanoha, Chiba 277-8561, Japan*

[5]*Institute for Solid State Physics, University of Tokyo, Kashiwanoha 5-1-5, Chiba 277-8581, Japan*

[6]*Department of Physics, University of Tokyo, Hongo, Tokyo 113-0033, Japan*

[7]*Canadian Light Source, Saskatoon, Saskatchewan S7N 2V3, Canada*

[8]*Department of Physics, Okayama University, Okayama 700-8530, Japan*

(Received 19 May 2014; revised manuscript received 13 July 2014; published 7 August 2014)

The coupled electronic-structural modulations of the ligand states in $IrTe_2$ have been studied by x-ray absorption spectroscopy and resonant elastic x-ray scattering (REXS). Distinctive preedge structures are observed at the Te-$M_{4,5}$ ($3d \rightarrow 5p$) absorption edge, indicating the presence of a Te $5p$–Ir $5d$ covalent state near the Fermi level. An enhancement of the REXS signal near the Te $3d \rightarrow 5p$ resonance at the $Q=(1/5,0,-1/5)$ superlattice reflection is observed below the structural transition temperature $T_s \sim 280$ K. The analysis of the energy-dependent REXS line shape reveals the key role played by the spatial modulation of the covalent Te $5p$–Ir $5d$ bond density in driving the stripelike order in $IrTe_2$, and uncovers its coupling with the charge and/or orbital order at the Ir sites. The similarity between these findings and the charge-ordering phenomenology recently observed in the high-temperature superconducting cuprates suggests that the iridates may harbor similar exotic phases.

DOI: 10.1103/PhysRevB.90.081104 PACS number(s): 71.45.Lr, 78.70.Ck, 78.70.Dm, 71.20.Be

Transition-metal compounds exhibit surprisingly rich electronic and magnetic properties due to the partially filled d orbitals. The fundamental properties of the electronic structure of transition-metal compounds can be described within the Zaanen-Sawatzky-Allen scheme. This differentiates between the Mott-Hubbard regime ($U < \Delta$) and the charge-transfer regime ($\Delta < U$), depending on the relative balance of the on-site Coulomb interaction U between the d electrons and the charge-transfer energy Δ between the ligand states and the transition-metal d states [1]. When Δ approaches zero, the ligand states are almost degenerate in energy with the transition-metal d levels. As a result, the ligand states may participate in those spin, charge, and/or orbital ordering phenomena that are peculiar to the correlated nature of the d orbitals. As an example of such phenomenology, ordering of the oxygen $2p$ holes is realized in the stripe-ordered phase of layered cuprates [2–6], or in the ladder-type Cu oxides [7].

Very recently, a first-order structural transition was discovered in the $5d$ transition-metal chalcogenide $IrTe_2$ at $T_s \sim 280$ K. This attracted great interest due to the concomitant discovery of superconductivity in the Pt- and Pd-substituted or intercalated compounds [8,9]. Clarifying the origin of the structural phase transition might be a critical step towards the understanding of superconductivity itself; however, to date several mechanisms have been debated, with a universal consensus still lacking. The phase transition is accompanied by the emergence of a superstructure lattice modulation in electron diffraction [9], with wave vector $Q=(1/5,0,-1/5)$ as expressed in reciprocal lattice units in tetragonal notation, which is here illustrated in Fig. 1. The main elements are the Ir-Ir dimerization along the a axis with period $5a$, and the consequent distortion of the triangular Ir sublattice in the a-b plane, conflating to an overall trigonal-to-triclinic symmetry reduction. The Ir-Ir dimerization likely stabilizes a unique stripelike order, with stripes running along the b axis, as indicated by x-ray diffraction [10,11] and extended x-ray absorption fine structure [12] studies. Such superstructure can be explained by the emergence of a charge-density wave (CDW) driven by perfect or partial nesting of the multiband Fermi surface [9]. Since in $IrTe_2$ the formal valence of Ir is +4, the Ir $5d$ electrons with t_{2g}^5 configuration are the closest to the chemical potential, and are thus expected to play a central role in a CDW. However, a photoemission study has shown that the charge-transfer energy Δ in $IrTe_2$ is close to zero, and that the Te $5p$ states are also important for the low-energy physics [13]. As further emphasized by recent studies [14–16], the Te $5p$ states might possibly be even more important than the Ir $5d$ states in the CDW phase transition of $IrTe_2$.

To resolve the controversy on the microscopic origin of the phase transition, the contribution of the Te $5p$ states to the superstructure formation must be experimentally quantified. In this context, resonant elastic x-ray scattering (REXS) experiments at the Te $3d \rightarrow 5p$ resonance represent the most effective method to directly probe the spatial ordering of the Te $5p$ states. Here we use REXS on $IrTe_2$ to reveal a modulation of the Te $5p$–Ir $5d$ covalent-bond state with the same wave vector $Q=(1/5,0,-1/5)$ as observed for the structural transition. This covalent-bond modulation is further coupled with the $5d$ orbital states at the Ir sites, and is thus ultimately responsible for the stripelike ordering formation in $IrTe_2$.

*ktakubo@issp.u-tokyo.ac.jp
†mizokawa@k.u-tokyo.ac.jp
‡damascelli@physics.ubc.ca

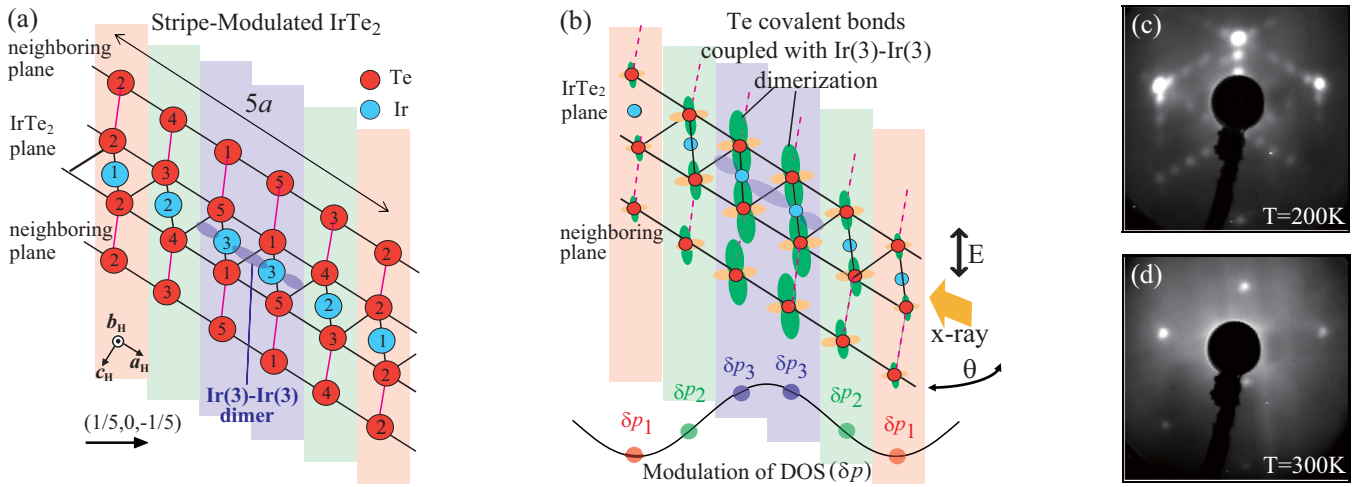

FIG. 1. (Color online) (a) $IrTe_2$ superstructure modulation with wave vector $Q=(1/5,0,-1/5)$, as expressed in reciprocal lattice units in tetragonal notation. Numeric labels denote the inequivalent Ir and Te sites. The modulation of the density of states (DOS), as estimated from dynamical mean-field theory (DMFT) [10] and highlighting the Ir(3)-Ir(3) dimerization, is shown at the bottom as well as above with correspondingly colored shading. (b) Illustration of the covalent bonds between the hybridized Te and Ir sites: the orbital size denotes the covalent character. By virtue of the experimental geometry (see text for detailed discussion), REXS is sensitive to these covalent bonds. (c), (d) LEED pattern measured on $IrTe_2$ at a temperature of 200 and 300 K, with 80 eV electrons.

REXS and x-ray absorption spectroscopy (XAS) measurements were performed at the REIXS beamline of the Canadian Light Source [17]. Single crystals of $IrTe_2$ were prepared using a self-flux method [14,18], and then cleaved *in situ* in ultra-high vacuum to minimize surface contamination effects. For the REXS measurements, the incident light was polarized along the (1,0,−1) direction [Fig. 1(b)]. XAS was used to determine the photoabsorption coefficient $\mu(\omega)$, which is proportional to the imaginary part of the form factor, $\mu(\omega)\propto \mathrm{Im}\{f_j(\hbar\omega)\}$. Low-energy electron diffraction (LEED) measurements were performed at University of British Columbia (UBC), with a SPECS ErLEED 100 setup and an electron energy of 80 eV, at a temperature of 200 and 300 K.

The $IrTe_2$ XAS spectra around the Te-$M_{4,5}$ edges (corresponding to the creation of a Te-3d core hole) are plotted in Fig. 2(a). Distinct preedge (labeled as $M_{4,5}$) and main edge structures can be clearly observed [19]. While the final state of the larger main edge is the s-d-f hybrid band (of 6s, 4f, and 5d character), the final state for the preedges is the Te-5p manifold. In light of previous experimental studies of these absorption channels [20–22], the preedge peak structure may be more precisely ascribed to transitions into Te-Ir covalent states. For a more conclusive assignment, in Fig. 2(b) we compare the preedge region for FeTe, $IrTe_2$, and $AuTe_2$ (which is iso-structural to $IrTe_2$). The preedge intensity increases in going from FeTe, to $IrTe_2$, and eventually to $AuTe_2$, contrary to the expectation that the number of absorption channels—and thus the XAS intensity—should be larger for lower d-shell occupation [23]. Here we argue that the growing intensity trend observed in Fig. 2(b) reflects an increase in covalence between ligand and transition-metal ions. The degree of covalence—dependent on the charge-transfer energy Δ—is expected to become larger for later transition metals and higher valences, consistent with the observed evolution of the Te-$M_{4,5}$ preedge structure. This is similar to the intensity evolution of the oxygen K-edge prepeak structure in transition-metal oxides, which is proportional to the unoccupied density of states (DOS) of the coupled ligand-oxygen-2p and transition-metal-d orbitals.

Figure 2(c) shows the Te-M_5 preedge spectra taken at 200 and 300 K. Light polarization was set parallel to the (1,0,0) axis; however, in general no polarization dependence of the XAS signal was observed. As evidenced by these results, the Te-site partial DOS around the Fermi level E_F, corresponding to a photon energy of ∼569.7 eV in XAS [24], is suppressed below the structural transition temperature T_s. At the same time, the partial DOS from 0.6 to 2.3 eV above E_F (corresponding to 570.3–572.0 eV in XAS) increases below T_s. As for the partial DOS above 2.3 eV (above 572.0 eV in XAS), and associated with the Te states hybridized with the Ir-e_g manifold, it does not show a pronounced temperature dependence. The spectral changes observed across the transition, i.e., the disappearance of the DOS dip in the range 0.6–2.3 eV above E_F, seem consistent with the result of band structure calculations and dynamical mean-field theory (DMFT) [10,11], as well as with recent angle-resolved photoemission spectroscopy (ARPES) and resonant inelastic x-ray scattering (RIXS) studies of $IrTe_2$ [16,25]. These results suggest a Rice-Scott saddle-point-driven CDW instability [26–28] associated with a Te-5p van Hove singularity at E_F, which in the low-temperature (LT) phase is removed from E_F due to the reconstruction of the electronic structure. The present XAS results for the unoccupied DOS are partly consistent with the ARPES/RIXS observations. However, the drastic change in the unoccupied DOS, taking place up to 2.3 eV above E_F, suggests that the simple saddle-point-driven CDW scenario is insufficient to fully describe the origin of the phase transition observed at $T_s \sim 280$ K.

Next, we discuss the superstructure peak observed in REXS at $Q=(1/5,0,-1/5)$ in the LT phase. Figure 3(a) shows a $(H,0,-L)$ momentum scan through the resonant peak at 200 K and at a photon energy of 571.3 eV, corresponding to the

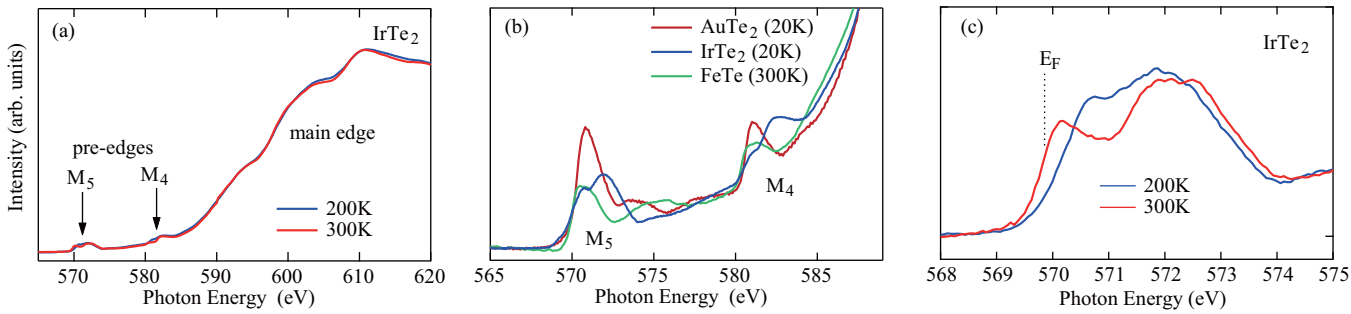

FIG. 2. (Color online) (a) $IrTe_2$ XAS spectra measured at the Te-M absorption edge at 200 and 300 K; the Te-$M_{4,5}$ preedge features are indicated by arrows. (b) Preedge XAS spectra from FeTe, $IrTe_2$, and $AuTe_2$. (c) $IrTe_2$ Te-M_5 XAS spectra measured at 200 and 300 K.

Te-M_5 prepeak position. The signal is resonantly enhanced in the XAS preedge region, as evidenced by the REXS photon-energy dependence shown in Figs. 3(c) and 3(d), indicating the active role of the covalent Te $5p$ –Ir $5d$ bond density in the CDW formation (the dip features found before the $M_{4,5}$ preedge structures will be analyzed in more detail in the discussion of Fig. 4). As for the XAS main-edge region, x-ray absorption fine structure oscillatory behavior is observed, likely originating from local scattering of photoelectrons; however, the main-edge scattering intensity lacks a resonant character, which indicates that the s-d-f hybrid band manifold does not participate in the ordering mechanism.

Figure 3(b) shows the detailed temperature dependence of the $Q=(1/5,0,-1/5)$ superstructure peak amplitude in REXS, measured across T_s during both cooling and warming cycles. The signal shows a sharp onset at T_s, consistent with the first-order character of the phase transition at ∼280 K. In addition, a clear hysteretic behavior is also observed (the presence of a hysteretic behavior in XAS is discussed in the Supplemental Material [29]). This points to the formation of a multidomain structure, where the CDW distortion—and in particular the shortening of one of the sides of the equilateral triangles forming the Ir sublattice in the a-b plane—may occur along any of the three triangular axes. The matching REXS intensity observed for the "slow" cooling and warming cycles in Fig. 3(b), and conversely the mismatch and complex time and temperature evolution observed for "fast" cooling runs (see Supplemental Material [29]), suggest the presence of a "glassy" domain evolution that can reach equilibrium between the three possible domain orientations only during slow temperature cycles [30]. This scenario is confirmed by LEED measurements on the very same sample which show—along all three axes defining the triangular Ir sublattice—analogous $(h/5,0,-L)$ superstructure reflections at 200 K [Fig. 1(c)], but not at 300 K [Fig. 1(d)]. This domain structure, and its complex glassy evolution, might explain the controversy in the determination of the LT-phase structure [9–11,31].

Finally, we discuss the energy-dependent REXS line shape shown in Figs. 3(c) and 3(d). One should note that E_F at ∼569.7 eV is located below the dip structure, while the resonant enhancement is maximum around 1 eV above E_F. Therefore, the partial Te-DOS at E_F contributes only weakly to the resonant enhancement seen in REXS, which instead mainly arises from the modulation of the unoccupied DOS around 1 eV for the five structurally inequivalent sites [Fig. 1(a)]. This result again challenges the conventional Fermi surface nesting picture as well as a van Hove singularity scenario, and instead agrees well with the results of band structure and DMFT calculations for the LT phase [10,11]. In particular in the DMFT calculations by Toriyama *et al.* [11], the partial DOS of the Te(1)-p_z orbital, which is hybridized with the dimerized Ir(3)-Ir(3) states, has indeed a sharp structure at around ∼1 eV; conversely, the DOS of Te(1)-$p_{x,y}$ and of all other Te-site p orbitals is suppressed in this region. An electronic modulation involving the Te $5p$ unoccupied DOS, coupled with the Ir site t_{2g}-orbital order, is the best candidate to explain the REXS results obtained in the LT phase.

For the quantitative analysis of the REXS line shape, we use a methodology similar to the one introduced for the case of stripe order in cuprates [6]. The model relies on XAS

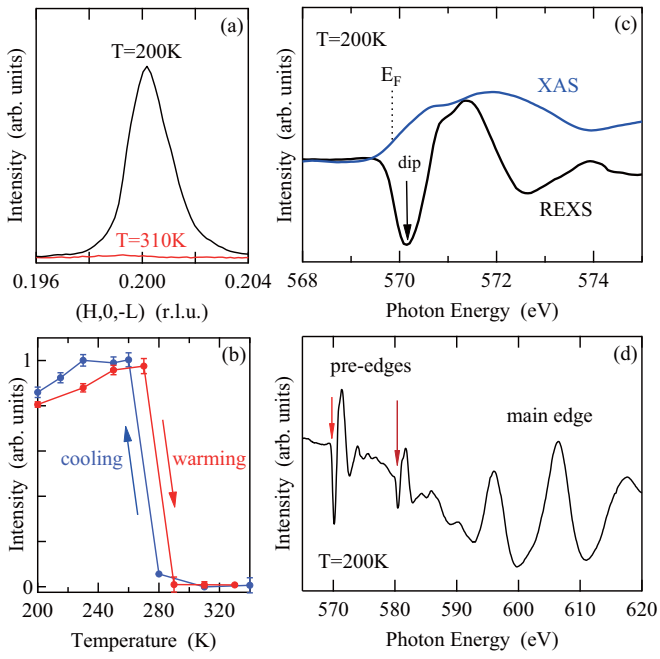

FIG. 3. (Color online) (a) REXS $(H,0,-L)$ scan through the $Q=(1/5,0,-1/5)$ superlattice peak measured on $IrTe_2$ at 200 and 310 K, with 571.3 eV photons. (b) Corresponding temperature dependence of the REXS intensity. (c) Comparison between REXS and XAS spectra measured in the M_5 preedge region at 200 K; the arrow marks the dip structure observed before the REXS enhancement. (d) REXS spectrum measured in the entire energy range of the Te-M edge x-ray absorption, at 200 K.

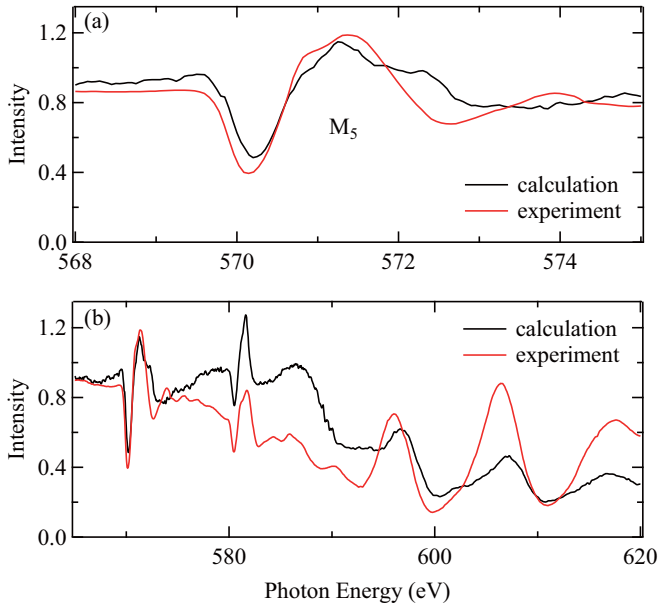

FIG. 4. (Color online) Calculated REXS intensity for the combination of a valence-modulation model (resonant term) with nonresonant lattice displacements, shown for (a) the M_5 preedge region and (b) the extended spectrum together with the experimental data.

measurements to determine the form factor $f(\omega)$ for the different Te sites (whereby any site-independent contribution will cancel out in REXS). The wave-vector ($\mathbf{Q}$) and photon-energy (ω) dependent structure factor $S(\mathbf{Q},\omega)$ is subsequently constructed based on the spatial modulation of $f(\omega)$ at the different atomic positions $\mathbf{r}_j$:

$$S(\mathbf{Q},\omega) = \sum_j f_j(\omega) e^{-i\mathbf{Q}\cdot\mathbf{r}_j}. \quad (1)$$

The experimental result is compared to three model calculations, where the major contribution to $S(\mathbf{Q},\omega)$ comes from, respectively, (i) lattice displacements, $\mathbf{r}_j = \mathbf{r}_j^0 + \delta\mathbf{r}_j$, where small displacements are used for the Te and Ir lattice sites in the supermodulated structure; (ii) energy shifts, $f_j(\omega) = f(\omega + \delta\omega_j)$, where $\delta\omega_j$ is the spatial modulation of the energy of the Te-5p state; and (iii) valence modulations, $f_j(\omega) = f(\omega, p + \delta p_j)$, where δp_j is the variation in the local valence of the Te ions (further details on the three model calculations are given in the Supplemental Material [29]). The best agreement for the sharp dip features on the preedges, as well as the high-energy oscillatory behavior, is obtained using the valence (local DOS) modulation model, involving the covalent bonds between Te and Ir in the outermost shells. The comparison with experimental data is shown in Fig. 4. Here, the form factors $f(\omega, p + \delta p_j)$ are assumed to modulate spatially as illustrated in the lower part of Fig. 1. Proper atomic displacements, contributing to the nonresonant terms, are also embedded in the structure factor calculations. The present valence-modulation model reflects the periodic modulation of the Te 5p orbitals coupled with the charge and/or orbital order at the Ir sites [Figs. 1(a) and 1(b)], similar to the case of stripe order in cuprates [2–6]. Furthering this similarity, the $IrTe_2$ doping-pressure phase diagram exhibits a competitive interplay between superconductivity and other ordered phases [8,9,14,32–35]; in analogy with recent studies of underdoped high-T_c cuprates [36–39], the role of stripe order as a candidate competing phase to superconductivity in $IrTe_2$ may also be probed—across the superconducting transition—by means of REXS at the Te $3d \rightarrow 5p$ resonance.

In conclusion, we have studied the ligand electronic states of $IrTe_2$ by XAS and REXS at the Te-$M_{4,5}$ edge. The distinct preedge structure at the Te-$M_{4,5}$ edge in XAS reveals the prominent covalent Te 5p-Ir 5d character of the near E_F electronic structure (with ligand holes on the Te 5p orbitals). A clear enhancement of REXS intensity at the $Q = (1/5, 0, -1/5)$ superlattice reflection is observed below $T_s \sim 280$ K. We find the spatial modulation of the unoccupied DOS at Te sites—covalently bonded to the Ir t_{2g} orbitals—to be responsible for the dominant contribution to the REXS intensity and, ultimately, for the stripelike ordering formation in $IrTe_2$.

We gratefully acknowledge M. Kobayashi for valuable discussions. This work was supported by the Max Planck–UBC Centre for Quantum Materials, the Killam, Alfred P. Sloan, Alexander von Humboldt, and NSERC's Steacie Memorial Fellowship Programs (A.D.), the Canada Research Chairs Program (A.D. and G.A.S.), NSERC, CFI, and CIFAR Quantum Materials. Part of the research described in this Rapid Communication was performed at the Canadian Light Source, which is funded by the CFI, NSERC, NRC, CIHR, the Government of Saskatchewan, WD Canada, and the University of Saskatchewan (Proposal No. 18-5295).

[1] J. Zaanen, G. A. Sawatzky, and J. W. Allen, Phys. Rev. Lett. **55**, 418 (1985).

[2] P. Abbamonte, A. Rusydi, S. Smadici, G. D. Gu, G. A. Sawatzky, and D. L. Feng, Nat. Phys. **1**, 155 (2005).

[3] J. Fink, E. Schierle, E. Weschke, J. Geck, D. Hawthorn, V. Soltwisch, H. Wadati, H.-H. Wu, H. A. Dürr, N. Wizent, B. Büchner, and G. A. Sawatzky, Phys. Rev. B **79**, 100502(R) (2009).

[4] J. Fink, V. Soltwisch, J. Geck, E. Schierle, E. Weschke, and B. Büchner, Phys. Rev. B **83**, 092503 (2011).

[5] D. G. Hawthorn, K. M. Shen, J. Geck, D. C. Peets, H. Wadati, J. Okamoto, S.-W. Huang, D. J. Huang, H.-J. Lin, J. D. Denlinger, R. Liang, D. A. Bonn, W. N. Hardy, and G. A. Sawatzky, Phys. Rev. B **84**, 075125 (2011).

[6] A. J. Achkar, F. He, R. Sutarto, J. Geck, H. Zhang, Y.-J. Kim, and D. G. Hawthorn, Phys. Rev. Lett. **110**, 017001 (2013).

[7] P. Abbamonte, G. Blumberg, A. Rusydi, A. Gozar, P. G. Evans, T. Siegrist, L. Venema, H. Eisaki, E. D. Isaacs, and G. A. Sawatzky, Nature (London) **431**, 1078 (2004).

[8] S. Pyon, K. Kudo, and M. Nohara, J. Phys. Soc. Jpn. **81**, 053701 (2012).

[9] J. J. Yang, Y. J. Choi, Y. S. Oh, A. Hogan, Y. Horibe, K. Kim, B. I. Min, and S.-W. Cheong, Phys. Rev. Lett. **108**, 116402 (2012).

[10] G. L. Pascut, K. Haule, M. J. Gutmann, S. A. Barnett, A. Bombardi, S. Artyukhin, T. Birol, D. Vanderbilt, J. J. Yang, S.-W. Cheong, and V. Kiryukhin, Phys. Rev. Lett. **112**, 086402 (2014).

[11] T. Toriyama, M. Kobori, Y. Ohta, T. Konishi, S. Pyon, K. Kudo, M. Nohara, K. Sugimoto, T. Kim, and A. Fujiwara, J. Phys. Soc. Jpn. **83**, 033701 (2014).

[12] B. Joseph, M. Bendele, L. Simonelli, L. Maugeri, S. Pyon, K. Kudo, M. Nohara, T. Mizokawa, and N. L. Saini, Phys. Rev. B **88**, 224109 (2013).

[13] D. Ootsuki, Y. Wakisaka, S. Pyon, K. Kudo, M. Nohara, M. Arita, H. Anzai, H. Namatame, M. Taniguchi, N. L. Saini, and T. Mizokawa, Phys. Rev. B **86**, 014519 (2012).

[14] A. F. Fang, G. Xu, T. Dong, P. Zheng, and N. L. Wang, Sci. Rep. **3**, 1153 (2013).

[15] Y. S. Oh, J. J. Yang, Y. Horibe, and S.-W. Cheong, Phys. Rev. Lett. **110**, 127209 (2013).

[16] T. Qian, H. Miao, Z. J. Wang, X. Liu, X. Shi, Y. B. Huang, P. Zhang, N. Xu, P. Richard, M. Shi, M. H. Upton, J. P. Hill, G. Xu, X. Dai, Z. Fang, H. C. Lei, C. Petrovic, A. F. Fang, N. L. Wang, and H. Ding, arXiv:1311.4946.

[17] D. G. Hawthorn, F. He, L. Venema, H. Davis, A. J. Achkar, J. Zhang, R. Sutarto, H. Wadati, A. Radi, T. Wilson, G. Wright, K. M. Shen, J. Geck, H. Zhang, V. Novk, and G. A. Sawatzky, Rev. Sci. Instrum. **82**, 073104 (2011).

[18] S. Pyon, K. Kudo, and M. Nohara, Physica C **494**, 80 (2013).

[19] The Ir-N edge absorption is not clearly seen in our spectra—which are thus dominated by the Te-$M_{4,5}$ edges—because the Ir $4p \rightarrow 5d$ transition matrix element is much smaller ($\sim$5%) than the one for the Te $3d \rightarrow 5p$ transition, due to the presence of radial nodes in the Ir $4p$ wave function.

[20] N. Jiang and J. C. H. Spence, Phys. Rev. B **70**, 014112 (2004).

[21] S. A. Song, W. Zhang, H. Sik Jeong, J.-G. Kim, and Y.-J. Kim, Ultramicroscopy **108**, 1408 (2008).

[22] D. Telesca, Y. Nie, J. I. Budnick, B. O. Wells, and B. Sinkovic, arXiv:1102.2155.

[23] Assuming a Te oxidation state of -2, the transition-metal valences are formally $Fe^{2+}(3d^6)$, $Ir^{4+}(5d^5)$, and $Au^{4+}(5d^7)$, which would suggest $AuTe_2$/FeTe/$IrTe_2$ as the sequence of progressively increasing intensity purely based on the filling of the transition-metal d orbitals.

[24] The Fermi level is located approximately around the middle of the absorption edge, with an accuracy of only about 0.2–0.3 eV; we note, however, that this uncertainty does not affect the following discussion.

[25] D. Ootsuki, S. Pyon, K. Kudo, M. Nohara, M. Horio, T. Yoshida, A. Fujimori, M. Arita, H. Anzai, H. Namatame, M. Taniguchi, N. L. Saini, and T. Mizokawa, J. Phys. Soc. Jpn. **82**, 093704 (2013).

[26] T. M. Rice and G. K. Scott, Phys. Rev. Lett. **35**, 120 (1975).

[27] R. Liu, W. C. Tonjes, V. A. Greanya, C. G. Olson, and R. F. Frindt, Phys. Rev. B **61**, 5212 (2000).

[28] T. Kiss, T. Yokoya, A. Chainani, S. Shin, T. Hanaguri, M. Nohara, and H. Takagi, Nat. Phys. **3**, 720 (2007).

[29] See Supplemental Material at http://link.aps.org/supplemental/10.1103/PhysRevB.90.081104 for methods, additional experimental data, and detailed calculations of the REXS intensity.

[30] We note that REXS and LEED, with their spot size of about 500 μm and 2 mm diameter, respectively, effectively average over the multidomain mosaic. Also, due to geometrical constraints of the sample manipulator, in REXS it was not possible to directly probe the superstructure wave vector along different directions; the presence of domains can thus be inferred only from the intensity evolution of the $Q = (1/5,0,-1/5)$ reflection.

[31] H. Cao, B. C. Chakoumakos, X. Chen, J. Yan, M. A. McGuire, H. Yang, R. Custelcean, H. Zhou, D. J. Singh, and D. Mandrus, Phys. Rev. B **88**, 115122 (2013).

[32] P.-J. Hsu, T. Mauerer, M. Vogt, J. J. Yang, Y. S. Oh, S-W. Cheong, M. Bode, and W. Wu, Phys. Rev. Lett. **111**, 266401 (2013).

[33] A. Kiswandhi, J. S. Brooks, H. B. Cao, J. Q. Yan, D. Mandrus, Z. Jiang, and H. D. Zhou, Phys. Rev. B **87**, 121107 (2013).

[34] M. Kamitani, M. S. Bahramy, R. Arita, S. Seki, T. Arima, Y. Tokura, and S. Ishiwata, Phys. Rev. B **87**, 180501 (2013).

[35] K. Kudo, M. Kobayashi, S. Pyon, and M. Nohara, J. Phys. Soc. Jpn. **82**, 085001 (2013).

[36] G. Ghiringhelli, M. Le Tacon, M. Minola, S. Blanco-Canosa, C. Mazzoli, N. B. Brookes, G. M. De Luca, A. Frano, D. G. Hawthorn, F. He, T. Loew, M. Moretti Sala, D. C. Peets, M. Salluzzo, E. Schierle, R. Sutarto, G. A. Sawatzky, E. Weschke, B. Keimer, and L. Braicovich, Science **337**, 821 (2012).

[37] R. Comin, A. Frano, M. M. Yee, Y. Yoshida, H. Eisaki, E. Schierle, E. Weschke, R. Sutarto, F. He, A. Soumyanarayanan, Yang He, M. Le Tacon, I. S. Elfimov, J. E. Hoffman, G. A. Sawatzky, B. Keimer, and A. Damascelli, Science **343**, 390 (2014).

[38] R. Comin, R. Sutarto, F. He, E. da Silva Neto, L. Chauviere, A. Frano, R. Liang, W. N. Hardy, D. Bonn, Y. Yoshida, H. Eisaki, J. E. Hoffman, B. Keimer, G. A. Sawatzky, and A. Damascelli, arXiv:1402.5415.

[39] R. Comin, R. Sutarto, E. H. da Silva Neto, L. Chauviere, R. Liang, W. N. Hardy, D. A. Bonn, F. He, G. A. Sawatzky, and A. Damascelli (unpublished).